Int. J. Electrochem. Sci., 8 **(2013)** 7581 - 7590

International Journal of
ELECTROCHEMICAL
SCIENCE
www.electrochemsci.org

Hydrothermal Preparation of Iron-Based Orthosilicate Cathode Materials with Different SiO_2 Particles and Their Electrochemical Properties

Dichang Xiao, Lianyi Shao, Rui Ma, Miao Shui, Jiqing Gao, Fengtao Huang, Kaiqiang Wu, Shangshu Qian, Dongjie Wang, Nengbing Long, Yuanlong Ren, Jie Shu[*]

Faculty of Materials Science and Chemical Engineering, Ningbo University, Ningbo 315211, Zhejiang Province, People's Republic of China
[*]E-mail: sergio_shu@hotmail.com; shujie@nbu.edu.cn

Received: 4 April 2013 / *Accepted:* 2 May 2013 / *Published:* 1 June 2013

Li_2FeSiO_4 and its derivates $Li_2Fe_{1-x}Mn_xSiO_4$ (x = 0.0, 0.2, 0.4, 0.6 and 0.8) are prepared by a simple hydrothermal reaction using $FeCl_2$•$4H_2O$, $MnCl_2$•$4H_2O$, LiOH•H_2O and SiO_2 as starting materials. During the sample preparation, the crystallite size of Li_2FeSiO_4 is controlled by the particle size of SiO_2 precursor. The as-prepared samples can be identified as orthorhombic phase with the space group of $Pmn2_1$, consisting of LiO_4 and FeO_4 tetrahedras linked to silicate $[SiO_4]^{4-}$ oxo-anions in distorted hexagonal packing of oxygen ions with half of tetrahedral sites taken by Li, Fe, and Si. Electrochemical results show that Li_2FeSiO_4 prepared with smaller SiO_2 particles shows higher reversible capacity and better cycle calendar life. The initial charge capacity and discharge capacity for Li_2FeSiO_4 prepared by 15 nm SiO_2 particles are 126.4 and 123.4 mAh/g, respectively. By replacement of Fe by Mn in the structure of Li_2FeSiO_4, a series of orthorhombic $Li_2Fe_{1-x}Mn_xSiO_4$ samples with x = 0.2, 0.4, 0.6 and 0.8 are hydrothermally prepared with 5 nm SiO_2 particles and compared with each other. As a result, Mn-doped $Li_2Fe_{1-x}Mn_xSiO_4$ samples show different variations on reversible capacity, capacity retention and cycling performance. It can be found that $Li_2Fe_{1-x}Mn_xSiO_4$ samples with low Mn doping content (x = 0.0 and 0.2) can improve the reversible lithium storage capacity and capacity retention ability of iron-based orthosilicates. Among all the compounds, $Li_2Fe_{0.8}Mn_{0.2}SiO_4$ can deliver the highest lithium storage capacity of 107.4 mAh/g with the corresponding capacity retention of 83.0 % after 20 cycles.

Keywords: Iron-based orthosilicates; Hydrothermal method; Cathode materials; Lithium-ion batteries

1. INTRODUCTION

Among all the known cathode materials, polyanion-type materials have been most widely studied as high capacity and high power cathode materials for lithium-ion batteries. Recent years,

lithium transition metal phosphates, $LiMPO_4$ (M=Fe, Mn, Ni, Co), have become the hottest research topics among all the polyanion-type cathode materials owing to outstanding structural stability and low cost [1-5]. However, lithium transition metal phosphates show low theoretical capacity (around 170 mAh/g) and low practical reversible capacity (about 160 mAh/g), which inhibit the large-scale application of phosphate-based rechargeable batteries in high performance energy storage field. For comparison, lithium transition metal orthosilicates, Li_2MSiO_4 (M=Fe, Mn, Ni, Co), show a larger theoretical capacity of 330 mAh/g as suitable high capacity cathode materials [6-10]. They also show splendid structural and thermal stabilities as promising high power cathode materials. Therefore, Li_2MSiO_4 may be potential cathode material for high performance energy storage and conversion devices.

For Li_2MSiO_4, the members Li_2NiSiO_4 and Li_2CoSiO_4 show high cost for the use of expensive metals Ni and Co. It makes Li_2NiSiO_4 and Li_2CoSiO_4 have high price with that of commercial $LiCoO_2$ and $LiNiO_2$. Furthermore, the delithiation potentials (>4.6 V) of Li_2NiSiO_4 and Li_2CoSiO_4 are too high to make the present electrolyte as suitable lithium ion diffusion medium for lithium-ion batteries. Besides, Li_2NiSiO_4 and Li_2CoSiO_4 show poor delithiation-lithiation kinetics property during charge-discharge process [6, 11-13]. Thus, Li_2NiSiO_4 and Li_2CoSiO_4 are unsuitable as cathode materials at the present stage.

In contrast, Li_2FeSiO_4 and Li_2MnSiO_4 are inexpensive cathode materials with the use of low cost and high abundance metals Fe and Mn. Although the theoretical capacity is 333 mAh/g based on the total delithiation of 2 Li per formula, Li_2FeSiO_4 can only deliver a reversible capacity of 150-160 mAh/g at the most time with the valence conversion between Fe^{2+} and Fe^{3+} [14-16]. Due to poor kinetics behavior, it is also difficult for Li_2MnSiO_4 to deliver a high reversible capacity close to the theoretical capacity of 333 mAh/g. The practical lithium storage capacity of Li_2MnSiO_4 is about 150-180 mAh/g [17-19], which is almost the same value as the one revealed by Li_2FeSiO_4. Most recently, Chen *et al* reported a hierarchical porous Li_2FeSiO_4/C composite by using in situ template synthesis, which can show a high reversible lithium storage capacity of 254 mAh/g [20]. By fabricating ultrathin nanosheets, Li_2FeSiO_4 can deliver a superior high reversible capacity of 340 mAh/g as reported by Rangappa [21]. It suggests that Li_2FeSiO_4 or Li_2MnSiO_4 can deliver a high lithium storage capacity with proper structure and particle size. In this work, we prepare Li_2FeSiO_4 and its derivates $Li_2Fe_{1-x}Mn_xSiO_4$ by a simple hydrothermal technique with different SiO_2 precursors. The electrochemical properties of as-prepared samples are carefully characterized with various physical and electrochemical measurements.

2. EXPERIMENTAL

2.1 Material Preparation and Characterization

Li_2FeSiO_4 and its derivates $Li_2Fe_{1-x}Mn_xSiO_4$ are prepared by hydrothermal reaction in Teflon-lined stainless steel autoclaves. The starting materials for hydrothermal preparation are $FeCl_2•4H_2O$, $MnCl_2•4H_2O$, $LiOH•H_2O$ and SiO_2 with particle sizes of 15 nm, 100 nm and 1 μm. The molar ratios of

Li:Fe:Mn:Si are 4:1:0:1 (Li_2FeSiO_4), 4:0.8:0.2:1 ($Li_2Fe_{0.8}Mn_{0.2}SiO_4$), 4:0.6:0.4:1 ($Li_2Fe_{0.6}Mn_{0.4}SiO_4$), 4:0.4:0.6:1 ($Li_2Fe_{0.4}Mn_{0.6}SiO_4$) and 4:0.2:0.8:1 ($Li_2Fe_{0.2}Mn_{0.8}SiO_4$). In the sample preparation, all the chemical reagents are purchased from Sinopharm Chemical Reagent Shanghai Co. Ltd.

Firstly, SiO_2 particles are dispersed and dissolved in LiOH solution. Secondly, the SiO_2-containing solution is added drop by drop into $FeCl_2$ or $FeCl_2$-$MnCl_2$ ethylene glycol solution. The final mixed solution are continuously stirred for 2 h and then put into Teflon-lined stainless steel autoclaves for hydrothermal reaction at 180 ℃ for 24 h. The resulting products are filtrated and washed by distilled water, and then dried at 80 ℃ for 12 h in a vacuum oven.

The powder XRD patterns of Li_2FeSiO_4 and its derivates $Li_2Fe_{1-x}Mn_xSiO_4$ are recorded by Bruker D8 Focus diffractometer using nickel-filtered Cu Kα radiation (0.15406 nm). The data are collected in a step scanning mode over the angular range between 10 and 65º with a constant counting time of 5 s per step. FTIR spectra of Li_2FeSiO_4 and its derivates $Li_2Fe_{1-x}Mn_xSiO_4$ powders are collected by Shimadzu infrared spectrophotometer with the wavenumber between 400 and 2000 cm^{-1}.

2.2 Battery Preparation and Characterization

For battery preparation, the working electrodes are composed of the mixture of 80 wt.% of as-prepared active materials, 10 wt.% of conductive carbon black and 10 wt.% of a polyvinylidene fluoride binder. Homogeneous slurry can be formed by adding N-methylpyrrolidine into the powder mixture. The working electrodes are prepared by casting the slurry on aluminum foil and drying in vacuum oven at 120 ℃ for 24 h, then cut into discs with a diameter of 15 mm. The active material loading is about 2-3 mg/cm^2 and the thickness of the film is about 35 μm.

Homemade two-electrode simulated testing batteries are fabricated by using active film as cathode, Whatman glass fiber filter as separator, metal lithium disc as anode and 1 mol/L $LiPF_6$ dissolved in a mixture of ethylene carbonate and dimethyl carbonate (1:1, v/v) as electrolyte in an Etelux Ar-filled glove box. All the charge/discharge cycles are recorded on multi-channel Land CT2001A battery testing systems at a rate of 0.05 C between 1.5 and 4.8 V in a constant temperature cabinet (25 ℃). Homemade three-electrode systems with the counter and reference electrodes of metal Li are used to perform electrochemical impedance spectroscopy (EIS) analysis. EIS patterns are collected on CHI 660D electrochemical workstation in the frequency range between 100000 and 0.01 Hz with an amplitude of 5 mV.

3. RESULTS AND DISCUSSION

Figure 1a shows the XRD patterns of Li_2FeSiO_4 prepared with different SiO_2 particles (15 nm, 100 nm and 1 μm). All the three patterns show the same Bragg positions. It can be found that there are eight sharp diffraction peaks appeared at 16.57, 24.64, 28.60, 33.15, 36.36, 38.03, 50.05 and 59.64º, corresponding to the (010), (011), (200), (210), (002), (211), (022) and (230) characteristic planes. The XRD patterns of the present samples can be identified as Li_2FeSiO_4 phase with the space group of $Pmn2_1$, consisting of a distorted hexagonal packing of oxygen ions with half of tetrahedral sites taken

by Li, Fe, and Si. No diffraction peak of unreacted starting materials, iron oxides or lithium silicate phases in the final products can be observed in the XRD patterns. These results are in good accordance with those data reported by Rangappa [21] and Nyten [22]. According to crystal structure of orthorhombic system, it is known that the structure of Li_2FeSiO_4 phase is isostructural with that of Li_3PO_4, consisting of infinite corrugated layers on the ac plane built by FeO_4 and SiO_4 tetrahedras, and linked by LiO_4 tetrahedras along the b-axis as the crystal structure shown in Figure 2.

Refined by Fullprof software, the lattice parameters of orthorhombic Li_2FeSiO_4 phases prepared by 15 nm, 100 nm and 1 μm SiO_2 powders are a = 6.256, b = 5.322 and c = 5.002 Å, a = 6.261, b = 5.328 and c = 5.011 Å, a = 6.269, b = 5.334 and c = 5.022 Å, respectively. The average crystallite size can be calculated from (210) peak by using Scherrer formula $d=k\lambda/\beta\cos\theta$, where d is the mean crystallite size, k is the constant parameter of shape factor (0.89), λ is the wavenumber of X-ray, β is the half maximum width of (210) peak and θ is the Bragg position of (210) peak. As a result, the average crystallite sizes of Li_2FeSiO_4 samples prepared by 15 nm, 100 nm and 1 μm SiO_2 particles are 8.4, 13.9 and 15.6 nm, respectively. Usually, smaller crystallite size will result in higher rate capability and higher reversible lithium storage capacity owing to short lithium ion diffusion pathways. Therefore, it is expected that Li_2FeSiO_4 samples prepared by 15 nm SiO_2 particles will show outstanding electrochemical properties.

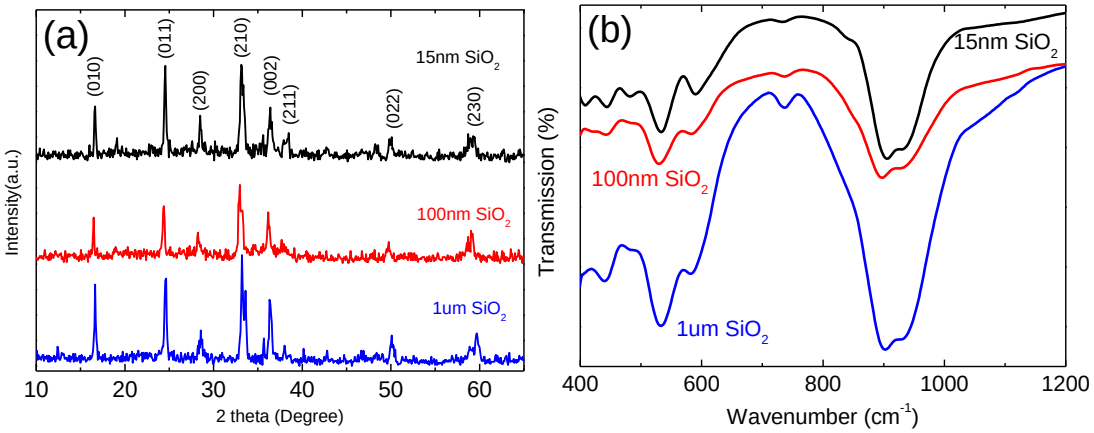

Figure 1. XRD patterns (a) and FTIR spectra (b) of Li_2FeSiO_4 prepared with different SiO_2 particles.

It is well-known that FTIR spectroscopy can show additional structure information of as-prepared Li_2FeSiO_4 phase. Here, the purpose of FTIR spectroscopy investigation is to study the short-range local environments of the Fe^{2+} in the distorted hexagonal packing of oxygen ions in the host Li_2FeSiO_4 lattices. The frequency of the infrared absorbed modes is always associated with the short-range local environment of oxygen coordination around the Fe^{2+} in the lattices, including the atomic motion of Fe^{2+}, crystal symmetry and the oxidation state of Fe^{2+}. The FTIR spectra of Li_2FeSiO_4 prepared by SiO_2 with particle sizes of 15 nm, 100 nm and 1 μm are shown in Figure 1b. It is clear that there are seven characteristic bands located at 935, 906, 735, 589, 533, 482 and 443 cm^{-1} for Li_2FeSiO_4 prepared by 15 nm SiO_2. The vibrational bands of as-prepared samples are in good accordance with those reported for Li_2FeSiO_4 and Li_2MnSiO_4 [23-26].

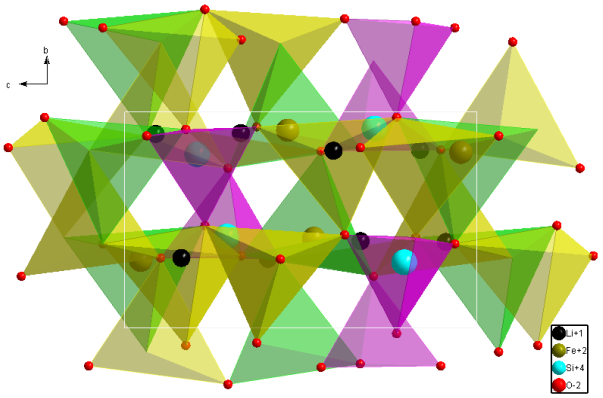

Figure 2. Crystal structure of Li_2FeSiO_4 with the space group of $Pmn2_1$.

As described by XRD patterns, the structure of Li_2FeSiO_4 is built from LiO_4 and FeO_4 tetrahedras linked to silicate $[SiO_4]^{4-}$ oxo-anions. Here, the IR-active modes of Li_2FeSiO_4 are mainly reflected by the characteristic vibrations of silicate tetrahedral $[SiO_4]^{4-}$ oxo-anions, which can be split into many bands owing to the correlation effects induced by the coupling of LiO_4 and FeO_4 tetrahedras in the crystal structure. The infrared bands at 935 and 896 cm^{-1} can be contributed to the stretching modes of Si-O bonds in SiO_4 tetrahedras. The absorption feature peak at 735 cm^{-1} is attributed to the bending vibration of Si-O-Si bridging bonds in SiO_4 tetrahedras. The FTIR bands at 589 and 533 cm^{-1} can be attributed to the bending vibration of Si-O bonds in SiO_4 tetrahedras. The infrared bands at 482 and 443 cm^{-1} involve the Li-O stretching modes in LiO_4 tetrahedras. For comparison, there are seven infrared modes appeared at 935, 896, 735, 585, 531, 479 and 446 cm^{-1} for Li_2FeSiO_4 prepared by 100 nm SiO_2, and seven vibrational peaks centered at 930, 903, 737, 583, 533, 482 and 441 cm^{-1} for Li_2FeSiO_4 prepared by 1 μm SiO_2. The shift of infrared bands can be obviously observed for the characteristic vibrations of Si-O and Li-O bonds as shown in Figure 1b. This distinct difference in frequencies of the infrared absorbed modes indicates the difference in microstructure and surface morphology of different Li_2FeSiO_4 samples prepared with different SiO_2 particles.

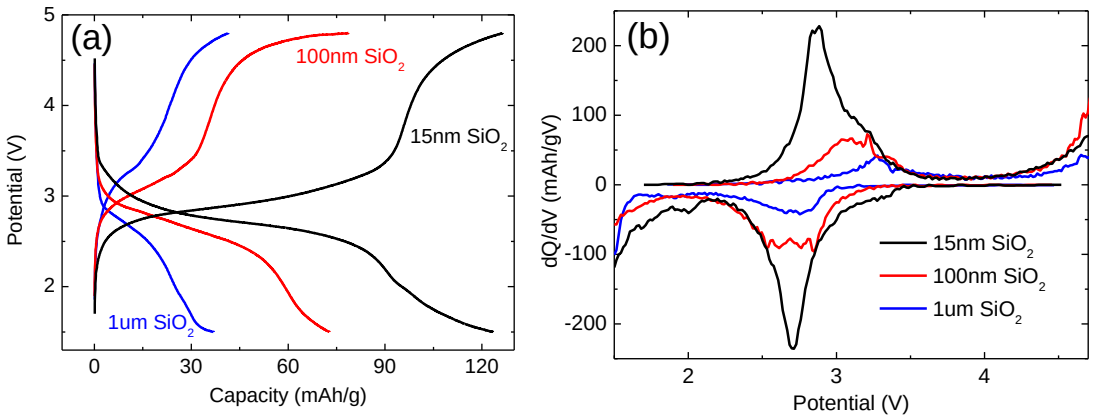

Figure 3. Charge-discharge curves and corresponding dQ/dV curves of Li_2FeSiO_4 prepared with different SiO_2 particles.

The charge-discharge curves and corresponding dQ/dV curves of Li_2FeSiO_4 prepared by SiO_2 particles with particle sizes of 15 nm, 100 nm and 1 μm are shown in Figure 3. Viewed from Figure 3a, it can be found that the main initial charge plateau is located at around 2.9 V and reverse discharge plateau is centered at 2.7 V for Li_2FeSiO_4 prepared by 15 nm SiO_2 particles. As a result, the average working potential is 2.8 V as the dQ/dV curves shown in Figure 3b. The initial charge capacity and discharge capacity for Li_2FeSiO_4 prepared by 15 nm SiO_2 particles are 126.4 and 123.4 mAh/g, respectively. These values are similar with those reported by other researchers [22-26], but much lower than the theoretical capacity of 333 mAh/g. In contrast, the initial charge curve of Li_2FeSiO_4 prepared by 100 nm SiO_2 particles can be divided into two plateaus located at 3.1 and 4.7 V corresponding to the delithiation capacities of 35 and 43.6 mAh/g. The delithiation potentials are much higher than those displayed by the sample prepared with 15 nm SiO_2 particles. However, only one reverse lithiation plateau appears at about 2.7 V. The reverse discharge capacity is 72.8 mAh/g, corresponding to 0.44 Li per formula storage in the structure. For Li_2FeSiO_4 prepared by 1 μm SiO_2 particles, two delithiation plateaus can be observed at 3.3 and 4.7 V, corresponding to the delithiation capacities of 20.5 and 21.0 mAh/g. The reverse discharge of Li_2FeSiO_4 prepared by 1 μm SiO_2 particles is about 37.1 mAh/g, which is much lower than the value (123.4 mAh/g) delivered by Li_2FeSiO_4 prepared by 15 nm SiO_2 particles. All these evidences suggest that Li_2FeSiO_4 prepared by smaller SiO_2 particles shows lower polarization and higher delithiation-lithiation capacity.

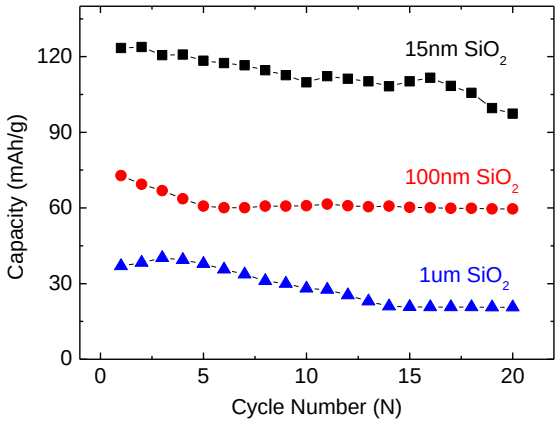

Figure 4. Cycling properties of Li_2FeSiO_4 prepared with different SiO_2 particles.

To investigate the cycling performance of Li_2FeSiO_4 samples prepared by SiO_2 particles with particle sizes of 15 nm, 100 nm and 1 μm, the capacity vs cycle number plots are shown in Figure 4. The homemade two-electrode simulated testing batteries are tested for 20 cycles at a rate of 0.05 C in a constant temperature cabinet (25 ℃). It can be found that the discharge capacity of Li_2FeSiO_4 prepared by 15 nm SiO_2 particles gradually decreases upon repeated cycles and shows a lithium storage value of 97.4 mAh/g after 20 cycles. The corresponding capacity retention is 78.9 %. In contrast, the 20^{th} discharge capacities of Li_2FeSiO_4 prepared by 100 nm and 1 μm SiO_2 particles are 59.6 and 20.6 mAh/g with the capacity retentions of 81.8 and 55.7 %, respectively. The enhanced lithium storage

capacity is probably attributed to small crystallite size and short lithium ion diffusion pathway as confirmed by XRD technique.

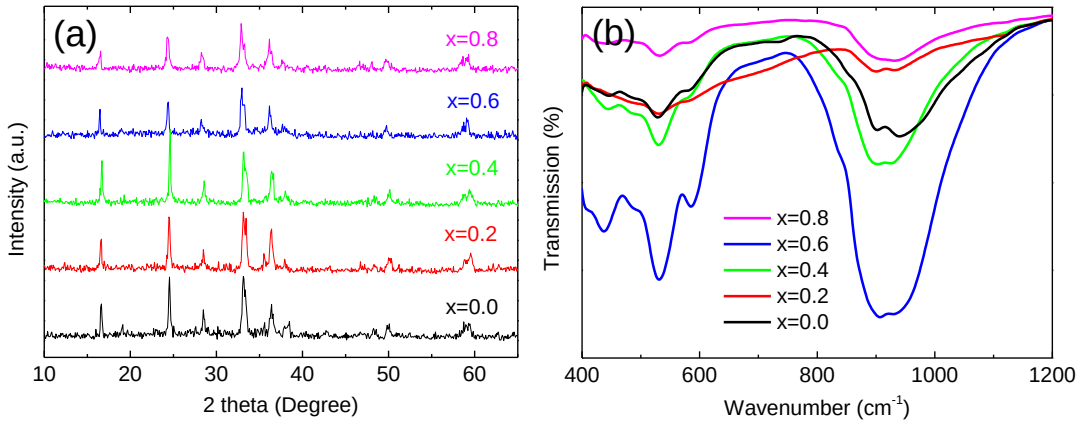

Figure 5. XRD patterns (a) and FTIR spectra (b) of $Li_2Fe_{1-x}Mn_xSiO_4$.

By doping Mn into the structure of iron-based orthosilicates, a series of $Li_2Fe_{1-x}Mn_xSiO_4$ samples with x = 0.2, 0.4, 0.6 and 0.8 are hydrothermally prepared with 5 nm SiO_2 particles and shown in Figure 5. As shown by the XRD patterns in Figure 5a, all the $Li_2Fe_{1-x}Mn_xSiO_4$ samples show the same crystal structure as that of Li_2FeSiO_4 phase with the space group of $Pmn2_1$, consisting of LiO_4, FeO_4 and MnO_4 tetrahedras linked to silicate tetrahedral $[SiO_4]^{4-}$ polyanions in distorted hexagonal packing of oxygen ions with half of tetrahedral sites occupied by Li, Fe, Mn, and Si atoms. These XRD patterns are in agreement with the previous reports of Li_2MnSiO_4 and $Li_2Fe_{1-x}Mn_xSiO_4$ [21, 27, 28]. No impurity of iron chlorides, manganese chlorides, iron oxides, manganese oxides or lithium silicate phases can be observed in the XRD patterns of as-prepared samples. As the XRD patterns shown in Figure 5a, it can be also observed that $Li_2Fe_{1-x}Mn_xSiO_4$ samples show similar lattice parameters with those of the pristine Li_2FeSiO_4 and the crystallite sizes of $Li_2Fe_{1-x}Mn_xSiO_4$ samples show no distinct evolution with the increase of Mn doping content.

The infrared spectra of $Li_2Fe_{1-x}Mn_xSiO_4$ samples with x = 0.0, 0.2, 0.4, 0.6 and 0.8 are shown and compared in Figure 5b. It is obvious that the stretching modes of Si-O bonds in SiO_4 tetrahedras show red-shift from 935 to 928 cm^{-1} and blue-shift from 896 to 907 cm^{-1} with the increase of Mn doping content. Moreover, the Li-O stretching mode in LiO_4 tetrahedras shows a red-shift from 443 to 436 cm^{-1} owing to the high Mn doping content. As well-known, the splitting vibrations of silicate tetrahedral $[SiO_4]^{4-}$ oxo-anions are mainly induced by the correlation effects of Li-O and M-O bonds in LiO_4 and MO_4 tetrahedras. Due to higher bond energy of Mn-O compared to Fe-O, the infrared bands of Mn-doped $Li_2Fe_{1-x}Mn_xSiO_4$ show an ordered shift based on the pristine Li_2FeSiO_4 sample.

A comparison of charge-discharge behaviors of pristine Li_2FeSiO_4 and Mn-doped $Li_2Fe_{0.2}Mn_{0.8}SiO_4$ is shown in Figure 6a. It can be found that $Li_2Fe_{0.2}Mn_{0.8}SiO_4$ sample shows a high delithiation plateau at around 4.5 V, corresponding to an initial charge capacity of 117.7 mAh/g. In the reverse discharge process, two lithiation plateaus can be observed at 2.55 and 1.75 V, corresponding to the discharge capacities of 48.6 and 46.9 mAh/g. The polarization between delithiation and lithiation processes is about 2.35 V, which is probably attributed to the high theoretical delithiation potential,

slow kinetics and poor electronic conductivity of $Li_2Fe_{1-x}Mn_xSiO_4$ samples as reported by Zhang [27] and Liu [29]. Based on the conversion reaction of Fe^{2+}/Fe^{3+} and Mn^{2+}/Mn^{3+} couples, the charge capacity at high delithiation plateau will increase and the charge capacity at low delithiation plateau will decrease with the increase of Mn doping content.

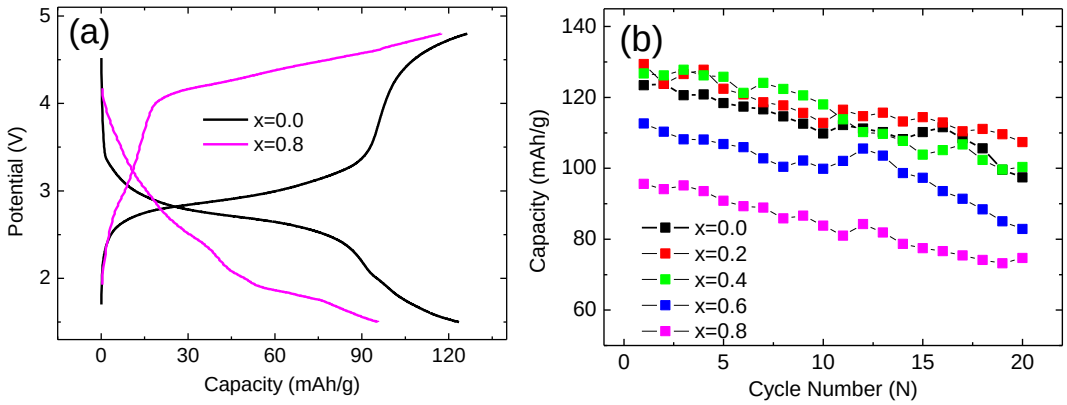

Figure 6. Charge-discharge curves and cycling properties of $Li_2Fe_{1-x}Mn_xSiO_4$.

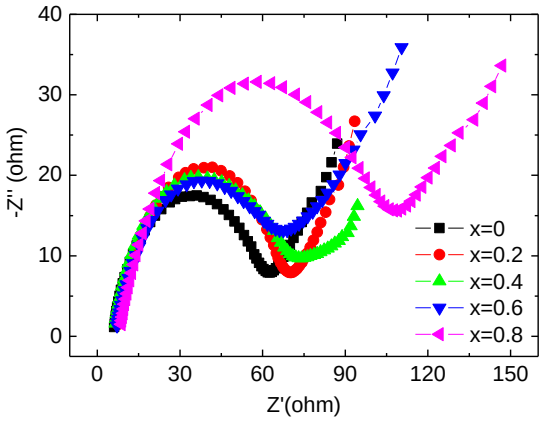

Figure 7. EIS spectra of $Li_2Fe_{1-x}Mn_xSiO_4$.

Figure 6b shows the capacity vs cycle number plots of $Li_2Fe_{1-x}Mn_xSiO_4$ samples with x = 0.0, 0.2, 0.4, 0.6 and 0.8. The initial discharge capacities of $Li_2Fe_{0.8}Mn_{0.2}SiO_4$, $Li_2Fe_{0.6}Mn_{0.4}SiO_4$, $Li_2Fe_{0.4}Mn_{0.6}SiO_4$ and $Li_2Fe_{0.2}Mn_{0.8}SiO_4$ are 129.4, 126.7, 112.6 and 95.6 mAh/g, respectively. After 20 cycles, the reversible lithium storage capacities of $Li_2Fe_{0.8}Mn_{0.2}SiO_4$, $Li_2Fe_{0.6}Mn_{0.4}SiO_4$, $Li_2Fe_{0.4}Mn_{0.6}SiO_4$ and $Li_2Fe_{0.2}Mn_{0.8}SiO_4$ are 107.4, 100.4, 82.8 and 74.7 mAh/g, respectively. Corresponding capacity retentions of $Li_2Fe_{0.8}Mn_{0.2}SiO_4$, $Li_2Fe_{0.6}Mn_{0.4}SiO_4$, $Li_2Fe_{0.4}Mn_{0.6}SiO_4$ and $Li_2Fe_{0.2}Mn_{0.8}SiO_4$ are 83.0, 79.2, 73.6 and 78.1 %, respectively. Seen from these electrochemical data, it is clear that low Mn doping content (x = 0.0 and 0.2) can improve the reversible lithium storage capacity and capacity retention ability of iron-based orthosilicates. These results are in accordance with the data described by EIS spectra as shown in Figure 7. EIS patterns show that $Li_2Fe_{1-x}Mn_xSiO_4$ samples with higher Mn doping content display poor electronic conductivity and slow kinetics for

charge transfer. As a result, $Li_2Fe_{0.2}Mn_{0.8}SiO_4$ shows the worst electrochemical properties but $Li_2Fe_{0.8}Mn_{0.2}SiO_4$ shows the best electrochemical properties among all the $Li_2Fe_{1-x}Mn_xSiO_4$ samples.

4. CONCLUSION

In this paper, $Li_2Fe_{1-x}Mn_xSiO_4$ samples with x = 0.0, 0.2, 0.4, 0.6 and 0.8 are hydrothermally synthesized and compared as cathode materials for lithium-ion batteries. The crystallite sizes of $Li_2Fe_{1-x}Mn_xSiO_4$ samples are carefully controlled by using SiO_2 particles with different particle sizes (15 nm, 100 nm and 1 μm). The as-prepared $Li_2Fe_{1-x}Mn_xSiO_4$ samples show orthorhombic phases (space group: $Pmn2_1$), which are isostructural with that of Li_3PO_4, consisting of infinite corrugated layers on the ac plane built by MO_4 and SiO_4 tetrahedras, and linked by LiO_4 tetrahedras along the b-axis. For Li_2FeSiO_4 prepared by 15 nm SiO_2 particles, it can be found that the charge plateau is located at around 2.9 V with the charge capacity of 126.4 mAh/g and reverse discharge plateau is centered at 2.7 V with the charge capacity of 123.4 mAh/g. The reversible discharge capacity is 97.4 mAh/g after 20 cycles with the corresponding capacity retention of 78.9 %. By using Mn doping in the structure, it is obvious that $Li_2Fe_{1-x}Mn_xSiO_4$ samples with low Mn content show improved reversibility and high reversible capacity but $Li_2Fe_{1-x}Mn_xSiO_4$ samples with high Mn content exhibit low reversible capacity. After 20 cycles, $Li_2Fe_{0.8}Mn_{0.2}SiO_4$ and $Li_2Fe_{0.6}Mn_{0.4}SiO_4$ can deliver reversible capacities of 107.4 and 100.4 mAh/g with corresponding capacity retentions of 83.0 and 79.2 %, respectively. It demonstrates that $Li_2Fe_{1-x}Mn_xSiO_4$ samples, especially for $Li_2Fe_{0.8}Mn_{0.2}SiO_4$, are promising cathode materials for lithium-ion batteries.

ACKNOWLEDGEMENTS

This work is sponsored by National 863 Program (2013AA050901), National Natural Science Foundation of China (No. 51104092) and Qianjiang Talent Project of Zhejiang Province (2011R10089). The work is also supported by K. C. Wong Magna Fund in Ningbo University, Open Foundation of State Key Laboratory of Materials Processing and Die & Mould Technology (2012-P01), Open Foundation of State Key Laboratory of Electronic Thin Films and Integrated Devices (KFJJ201209) and Open Foundation of State Key Laboratory Breeding Base of Green Chemistry-Synthesis Technology (GCTKF2012002).

References

1. A.K. Padhi, K. Nanjundaswamy, J.B. Goodenough, *J. Electrochem. Soc.*, 144 (1997) 1188-1194.
2. G. Kobayashi, S. Nishimura, M.S. Park, R. Kanno, M. Yashima, T. Ida, A. Yamada, *Adv. Funct. Mater.*, 18 (2008) 1-9.
3. T. Drezen, N.H. Kwon, P. Bowen, I. Teerlinck, M. Isono, I. Exnar, *J. Power Sources*, 174 (2007) 949-953.
4. N.N. Bramnik, K. Nikolowski, D.M. Trots, H. Ehrenbergb, *Electrochem. Solid-State Lett.*, 11 (2008) A89-A93.
5. J. Wolfenstine, J. Allen, *J. Power Sources*, 142 (2005) 389-390.
6. C. Lyness, B. Delobel, A.R. Armstrong, P.G. Bruce, *Chem. Commun.*, 46 (2007) 4890-4892.
7. L.M. Li, H.J. Guo, X.H. Li, Z.X.Wang,W.J. Peng, K.X. Xiang, X. Cao, *J. Power Sources*, 189

(2009) 45-50.
8. J. Liu, H.Y. Xu, X.L. Jiang, J. Yang, Y.T. Qian, *J. Power Sources*, 231 (2013) 39-43.
9. D. Santamaría-Pérez, U. Amador, J. Tortajada, R. Dominko, M.E. Arroyo-de Dompablo, *Inorg. Chem.*, 51 (2012) 5779-5786.
10. M.E. Arroyo-de Dompablo, M. Armand, J.M. Tarascon, U. Amador, *Electrochem. Commun.*, 8 (2006) 1292-1298.
11. Z.L. Gong, Y.X. Li, Y. Yang, *J. Power Sources*, 174 (2007) 524-527.
12. G.H. Zhong, Y.L. Li, P. Yan, Z. Liu, M.H. Xie, H.Q. Lin, *J. Phys. Chem. C*, 114 (2010) 3693-3700.
13. G. He, G. Popov, L.F. Nazar, *Chem. Mater.*, (2013) DOI:10.1021/cm302823f.
14. A. Nyten, A. Abouimrane, M. Armand, T. Gustafsson, J.O. Thomas, *Electrochem. Commun.*, 7 (2005) 156-160.
15. X.Z. Wu, X. Jiang, Q.S. Huo, Y.X. Zhang, *Electrochim. Acta*, 80 (2012) 50-55.
16. A.R. Armstrong, N. Kuganathan, M.S. Islam, P.G. Bruce, *J. Am. Chem. Soc.*, 133 (2011) 13031-13035.
17. S.H. Luo, M. Wang, W.N. Sun, *Ceram. Int.*, 38 (2012) 4325-4329.
18. F.Q. Wang, J. Chen, C. Wang, B.L. Yi, *J. Electroanal. Chem.*, 688 (2013) 123-129.
19. N. Kuganathan, M.S. Islam, *Chem. Mater.*, 21 (2009) 5196-5202.
20. Z.X. Chen, S. Qiu, Y.L. Cao, J.F. Qian, Xi.P. Ai, K. Xie, X.B. Hong, H.X.Yang, *J. Mater. Chem. A*, 1 (2013) 4988-4992.
21. D. Rangappa, K.D. Murukanahally, T. Tomai, A. Unemoto, I. Honma, *Nano Lett.*, 12 (2012) 1146-1151.
22. A. Nyten, A. Abouimrane, M. Armand, T. Gustafsson, J.O. Thomas, *Electrochem. Commun.*, 7 (2005) 156-160.
23. K. Zaghib, A.A. Salah, N. Ravet, A. Mauger, F. Gendron, C.M. Julien, *J. Power Sources*, 160 (2006) 1381-1386.
24. K. Gao, C.S. Dai, J. Lv, S.D. Li, *J. Power Sources*, 211 (2012) 97-102.
25. C. Deng, S. Zhang, Y. Gao, B. Wu, L. Ma, Y.H. Sun, B.L. Fu, Q. Wu, F.L. Liu, *Electrochim. Acta*, 56 (2011) 7327-7333.
26. S.H. Luo, M. Wang, W.N. Sun, *Ceram. Int.*, 38 (2012) 4325-4329.
27. S. Zhang, Y. Li, G.J. Xu, S.L. Li, Y. Lu, O. Toprakci, X.W. Zhang, *J. Power Sources*, 213 (2012) 10-15.
28. T. Muraliganth, K.R. Stroukoff, A. Manthiram, *Chem. Mater.*, 22 (2010) 5754-5761.
29. S.K. Liu, J. Xu, D.Z. Li, Y. Hu, X. Liu, K. Xie, *J. Power Sources*, 232 (2013) 258-263.